PCCP

PAPER

View Article Online
View Journal | View Issue

Cite this: *Phys. Chem. Chem. Phys.*, 2015, **17**, 13290

Hydrogen bonding motifs in a hydroxy-bisphosphonate moiety: revisiting the problem of hydrogen bond identification†

Mitra Ashouri,[a] Ali Maghari[a] and M. H. Karimi-Jafari*[b]

Received 3rd February 2015,
Accepted 14th April 2015

DOI: 10.1039/c5cp00693g

www.rsc.org/pccp

Bisphosphonates are important therapeutic agents in bone-related diseases and exhibit complex H-bonding networks. To assess the role of H-bonds in biophosphonate stability, a full conformational search was performed for methylenebisphosphonate (**MBP**) and 1-hydroxyethylidene-1,1-diphosphonate (**HEDP**) using the MP2 method in conjunction with the continuum solvation model. The most stable structures and their equilibrium populations were analyzed at two protonation states *via* assignment of H-bonding motifs to each conformer. Geometrical and topological approaches for the identification and characterization of H-bonds were compared with each other, and some of the important correlations between H-bond features were described over the entire conformational space of a hydroxy-bisphosphonate moiety. The topologically derived H-bond energy obtained from the local density of potential energy at bond critical points shows consistent correlations with other measures such as H-bond frequency shift. An inverse power form without an intercept predicts topological H-bond energies from hydrogen-acceptor distances with an RMS error of less than 1 kcal mol^{-1}. The consistency of this measure was further checked by building a model that reasonably reproduces the relative stabilities of different conformers from their hydrogen-acceptor distances. In all systems, the predictions of this model are improved by the consideration of weak H-bonds that have no bond critical point.

1. Introduction

Bisphosphonates (BP) are an important class of organophosphorous compounds with a wide range of applications from industrial to biomedical areas. In addition to their use as anti-corrosive or complexing agents, in recent decades, they have played an important role in the global pharmaceutical market in the treatment of a variety of bone-related diseases such as osteoporosis, Paget's disease and hypercalcemia due to malignancy.[1,2] The main biological targets of BPs are the minerals of bone and farnesyl pyrophosphate synthase (FPPS), a key enzyme of the mevalonate pathway.[3–6] The structures of BPs are characterized by a P–C–P backbone and two side chains on the C atom. Considerable efforts have been devoted over many years to modulate the activities of BPs by changing the structures of the side chains.[7,8] Methylenebisphosphonate (**MBP**) is the simplest form in which the two side chains are hydrogen atoms. Replacing them with an OH and a methyl group leads to 1-hydroxyethylidene-1, 1-diphosphonic acid (**HEDP**), which exhibits a considerably different biomedical activity. In the most potent bisphosphonates in clinical use, one of the side chains is a hydroxyl group, and the other is a bulky group with a nitrogen moiety either in an alkyl chain or within a heterocyclic structure. As polyprotic acids, all BPs have different protonation states at different pH values, and there are numerous sites in their structures that can act as donors and/or acceptors in complex intra- or intermolecular hydrogen bonding networks.[9] Accordingly, the hydrogen bonds play an important role in the conformational flexibility of BPs in aqueous media and in their interactions with biological targets.[10]

A few computational studies have been published on BPs.[11–16] Among them, some have focused on the interactions of BPs with cations or solvent molecules,[11,12] while others have tried to provide some insight into the interactions of BPs with biological targets.[13,14] Another notable theoretical study is a DFT modelling study of conformers of **HEDP** that complements the experimental analysis

[a] *Department of Physical Chemistry, School of Chemistry, College of Science, University of Tehran, Tehran, Iran*
[b] *Department of Bioinformatics, Institute of Biochemistry and Biophysics, University of Tehran, Tehran, Iran. E-mail: mhkarimijafari@ut.ac.ir; Fax: +98 (0)21 66404680; Tel: +98 (0)21 66969257*

† Electronic supplementary information (ESI) available: H-bond motifs, populations, relative energy terms, equilibrium constants and hydrogen bond properties of all conformers in HL and H2L forms of HEDP. Fitted functional forms, fit parameters and regression quality obtained between the best correlated features of H-bond. Benchmark calculations with correlation consistent basis sets. Distribution of all H-bonds in **MBP** and **HEDP** over geometrical parameters. See DOI: 10.1039/c5cp00693g

of pH-dependent conformers of this compound.[15] In that work, the computed Raman spectra of identified conformers of **HEDP** were used to assign the vibrational bands in experimental spectra. In a recent study,[16] the conformational space of pamidronate was analyzed with DFT and *ab initio* methods, and the most stable conformers of this compound were characterized based on their relative stabilities, equilibrium populations and intramolecular hydrogen bonds. It was shown that the geometrical and topological criteria for the identification of H-bonds provide the same results in most cases, but are in disagreement in some notable situations. The hydrogen bonds in a hydroxy-bisphosphonate subunit can be classified in two groups. The first group of H-bonds are those formed between phosphonate moieties, and the second type of bond is formed between hydroxyl and one of the two phosphonate groups. In this work, we aim to provide a more general analysis of H-bonding patterns and their implications for the conformational diversity of a hydroxy-bisphosphonate structural module. Indeed, a detailed conformational analysis of BPs is a perquisite to study their interactions with biological targets.

Different approaches are commonly used to estimate the existence and strength of H-bonds.[17–19] In the present study, we used simple geometrical criteria and more sophisticated criteria based on topology of electron density obtained from quantum theory of atoms in molecules (QTAIM). By testing these criteria against each other, we tried to determine the extent of agreement between the QTAIM criteria of H-bond formation and simple geometrical criteria. We also paid some attention to a more general question: to what extent is the qualitative and/or quantitative analysis of QTAIM results consistent with the relative stability of different conformers? Moreover, most of the applications of QTAIM have focused on the most stable structures of the considered compounds; there is less comparative information on the trend of results applied to numerous structures of a multi-conformer system. In this regard and in conjunction with the problem of H-bond characterization, it is interesting to check whether the empirical correlations obtained over the most stable structures of different compounds are still valid for different conformations of a single molecule.

2. Methodology

A hydroxy-bisphosphonate group (Fig. 1) is a polyprotic moiety. In its fully protonated form, there are five O–H bonds, of which four (P–O–H ones) are ionizable. The successive deprotonation of this tetraprotic acid results in different protonation states that will be denoted herein as $\mathbf{H_4L}$, $\mathbf{H_3L}$, $\mathbf{H_2L}$, **HL** and **L**, dropping the total charge in the notations. In the case of **HEDP**, measured values of 1.21, 2.55, 6.87 and 10.66 have been reported for pK_{a1} to pK_{a4}, respectively.[20] In this work, we focused on the $\mathbf{H_2L}$ and **HL** protonation states since the analysis of species distribution *via* NMR controlled titrations in ref. 20 shows that the solution of **HEDP** in pH = 7 is a mixture of these states with nearly equal mol fractions.

2.1. Conformational search

The conformational space of **MBP** and **HEDP** was explored by systematic variation of all rotatable bonds (red bonds in Fig. 1).

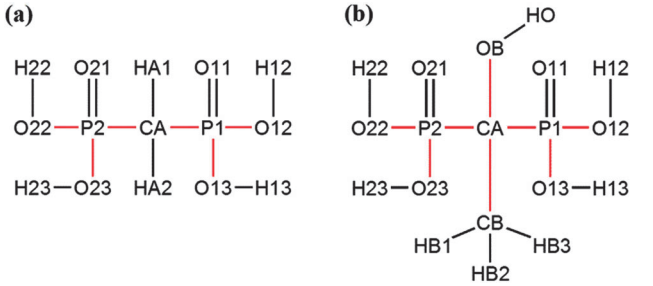

Fig. 1 Structures and atom naming of the fully protonated forms of **MBP** (a) and **HEDP** (b). Red bonds are explored in conformational searches.

All torsions containing hydrogen atoms were incremented in steps of 90°, while a 60° step size was used for others. All symmetrically unique structures were optimized at the HF/3-21G level of theory in conjunction with the conductor polarized continuum model (C-PCM)[21,22] for inclusion of solvation effects. All unique conformers at this level were then submitted for further optimization at the MP2/6-31++G(d,p) level of theory with inclusion of solvation effects *via* C-PCM. In the case of multi-H-bond systems, in which weaker intramolecular interactions play an important role in the conformational diversity of the system, the MP2 method is superior to DFT, although it is more expensive. In the same manner, HF/3-21G is preferred in this work over semiempirical methods for prescreening the conformational space. This resulted in 4, 8, 22 and 37 symmetrically unique conformers for **MBP-HL**, **MBP-H_2L**, **HEDP-HL** and **HEDP-H_2L**, respectively. At the same level of theory, normal mode analysis was performed on the final conformations to ensure their minimum energy character and also to obtain molecular partition functions and vibrational frequencies. It should be noted that the MP2 level of theory is not the ideal method to completely cover the dispersion contributions that seem to be dominant in the studied systems. However, to obtain more accurate relative energies, additional single-point energy calculations were performed at the MP2/6-311++G(2df,2p) level of theory.

To this point, all calculations were performed *via* the C-PCM continuum solvation model, including the electrostatic contribution to the solvation free energy. Additional C-PCM calculations were performed for cavitation, dispersion and repulsion contributions of solvation free energy. The cavitation energy was calculated by the method of Pierotti,[23] and the empirical method of Floris and Tomasi[24] was used for dispersion and repulsion contributions. In all C-PCM calculations, the FIXPVA tessellation method (fixed points with variable area) was used.[25] To obtain a more accurate gradient and smoother potential energy surface, the initial number of tesserae for each atomic sphere increased to 240. Accordingly, the calculated total free energy of each conformer can be expressed as:

$$G_{tot} = E_{tot} + G_{therm}^{MP2/BS1} \quad (1)$$

$$E_{tot} = E_{gas}^{MP2/BS2} + E_{ZPE}^{PCM\text{-}MP2/BS1} + \Delta G_{solv} \quad (2)$$

$$\Delta G_{solv} = \Delta G_{solv,els}^{PCM\text{-}MP2/BS2} + \Delta G_{solv,disp}^{PCM} + \Delta G_{solv,rep}^{PCM} + \Delta G_{solv,cav}^{PCM} \quad (3)$$

where G_{therm} is the thermal correction on free energy at 298.15 K, E_{gas} and E_{ZPE} are the gas phase electronic energy and its zero point

vibrational energy correction, respectively, and ΔG_{solv} is the total free energy of solvation obtained from the C-PCM model, including electrostatic ($\Delta G_{solv,els}$), cavitation ($\Delta G_{solv,cav}$), dispersion ($\Delta G_{solv,disp}$) and repulsion ($\Delta G_{solv,rep}$) contributions. BS1 and BS2 are the 6-31++G(d,p) and 6-311++G(2df,2p) basis sets, respectively. Calculated relative conformational energies might be the subject of basis set superposition error (BSSE).[26,27] It has been shown that the existence of BSSE can dramatically affect the relative energies of different conformers.[27] However, the BSSE will be diminished at the complete basis set (CBS) limit. In this regard, additional calculations were performed on some conformers of MBP to estimate the basis set-related errors in calculated MP2 gas-phase relative energies. The hierarchy of correlation consistent basis sets[28,29] denoted as cc-pVXZ and aug-cc-pVXZ (with X = D, T, Q) were used to estimate the CBS limit. Two different CBS estimations were provided based on augmented series. The first one, denoted as CBS1, was obtained *via* an exponential extrapolation scheme[30] using aug-cc-pVDZ, aug-cc-pVTZ and aug-cc-pVQZ values of HF energy in conjunction with an X^{-3} extrapolation scheme[31] using aug-cc-pVTZ and aug-cc-pVQZ values of correlation energy. The second estimate denoted as CBS2 was provided by separate $X^{-\gamma}$ extrapolation schemes[32] using HF (with γ = 3.4) and correlation (with γ = 2.2) energies obtained by aug-cc-pVDZ and aug-cc-pVTZ basis sets. All *ab initio* results were obtained by the GAMESS suite of programs.[33]

For each conformer, the equilibrium population was calculated according to standard techniques of statistical mechanics.[34,35] The lowest energy (E_{tot}) structure in each protonation form was kept as a reference ($C_{ref.}$), and according to the equation

$$C_{ref.} \Leftrightarrow C_i \quad K_i = \frac{[C_i]}{[C_{ref.}]}, \tag{4}$$

each conformer C_i was assumed to be in equilibrium with the reference conformer. The equilibrium constant K_i is given by the following equation:

$$K_i = \frac{q_i}{q_{ref.}} = K_i^{rot} K_i^{vib} K_i^{elec} = \frac{q_i^{rot}}{q_{ref.}^{rot}} \frac{q_i^{vib}}{q_{ref.}^{vib}} \frac{q_i^{elec}}{q_{ref.}^{elec}} \tag{5}$$

where q_i and $q_{ref.}$ are the molecular partition function of the ith and reference conformer, respectively. In this equation the equilibrium constant is factorized to the rotational (K^{rot}), vibrational (K^{vib}) and electronic (K^{elec}) contributions, and q^{rot}, q^{vib} and q^{elec} are the rotational, vibrational and electronic parts of the molecular partition function, respectively. The fraction of each conformer in the equilibrated sample was then obtained according to the following relation:

$$X_i = \frac{K_i}{\sum_i K_i} \tag{6}$$

where the sum in the denominator goes through all conformers including the reference one (note that $K_{ref.}$ = 1).

2.2. Hydrogen bond characterization

All hydrogen bonds in all located conformers were identified and characterized by geometrical and topological criteria. In the case of geometrical criteria, an H-bond was initially identified when the hydrogen–acceptor distance (R_{HA}) was less than the sum of van der Waals radii of these atoms, and the donor–hydrogen–acceptor angle (θ_{DHA}) was simultaneously larger than 100 degrees. These loose thresholds were then tightened by assessing the level of agreement with other criteria. Tabulated values by Bondi[36] were used as reference van der Waals radii. For identified H-bonds, the donor-hydrogen (R_{DH}) and donor–acceptor distances (R_{DA}) were also considered as characteristic geometrical parameters in subsequent analysis. On the other hand, the QTAIM was utilized to define an independent set of criteria based on the topological characteristics of the electron density.[37] An H-bond was identified topologically if there was a bond critical point (bc) between hydrogen and the acceptor atom. In this case, some topological characteristics were then calculated, including the electron density (ρ_{bc}), it's Laplacian (L_{bc}) and the density of potential energy (V_{bc}). Since a ring is created upon the formation of intramolecular H-bonds, a ring critical point (rc) appears in the electron density topology. A similar set of parameters (ρ_{rc}, L_{rc} and V_{rc}) were thus defined at this point as other topological characteristics of H-bonds. Finally, the empirically derived relation $E_{HB} \approx V_{bc}/2$ was used as a topological measure of the strengths of different H-bonds. This relation was derived from correlations investigated over a set of crystal structures.[38] QTAIM calculations were performed by the AIM2000 program.[39] In an assessment of different methods for estimating H-bond energies, a reasonable correlation has been obtained between the IR frequency shift of the donor-hydrogen stretching vibration and the H-bond energy.[19] Accordingly, the vibrational frequency shift ($\Delta\nu$) was used as a third independent measure to analyze the geometrical and topological criteria of H-bonds.

This pool of H-bond data provides an opportunity to obtain some insight into the following questions: (i) to what extent are the geometrical and topological criteria in agreement for the identification of H-bonds over the entire conformational space of a molecule? (ii) How do the topological and geometrical characteristics of H-bonds correlate with themselves and each other? (iii) Do the QTAIM-derived topological features of H-bonds provide predictive information about the relative stabilities of different conformers? In this regard, linear, reciprocal and logarithmic models were examined between the best correlated pairs of H-bond properties.

In each case, the goodness of the fit was measured by the coefficient of determination (r^2) and the root mean square error (RMSE) of the fitted models. To clarify the patterns of hydrogen bonding in a hydroxy-bisphosphonate moiety, simple graph-like representations were designed to introduce H-bond motifs. In each of these pictorial motifs, a triangle was used for a phosphonate group with different edge colors for protonated and bare oxygen atoms. The hydroxyl group of **HEDP** was represented by a circle, and H-bonds were denoted as arrows from donors to acceptors (see Table 2). Each of these graph-like representations will be referred to as an H-bond motif (denoted as **M1**, **M2**, **M3**... for each protonation state of **MBP** and **HEDP**), and some conformers might have the same motif. Thus, there is not a one-to-one relationship between conformation numbers and motif

numbers, although both of them are numbered in order of increasing energy.

3. Results and discussions

The calculated energetic and equilibrium quantities of all conformers of **HL** and **H_2L** forms of **MBP** and some low-lying conformers of **HEDP** can be found in Table 1. The full set of data is reported in the ESI† (Tables S1 and S2). The corresponding structures of these conformers are depicted in Fig. 2 after aligning them along their P–C–P backbones. In Table S6 (ESI†), the values of relative MP2 gas-phase energies of some selected **MBP** conformers are reported for correlation consistent basis sets and two CBS estimations. The aug-cc-pVTZ and aug-cc-pVQZ relative energies are very similar and nearly converged to CBS estimations of relative energies. An analysis of BSSE trends in normal alkanes of various sizes shows that the results of aug-cc-pVQZ could be considered as free of intramolecular BSSE.[27] The 6-311++G(2df,2p) values used in current study are within less than 0.5 kcal mol^{-1} of aug-cc-pVQZ and both CBS estimations. Accordingly, most of the conclusions drawn here from relative conformer energies are valid for the MP2 level of theory and are not considerably affected by basis set-related errors.

In Table 2, graph-like representations of different H-bonding motifs are listed for both **MBP** and **HEDP**. The geometrical and topological features of all identified **MBP** H-bonds can be found in Table 3. The full set of H-bond data for all conformers of **HEDP** can be found in ESI† (Tables S3 and S4). It would be informative to make a note regarding the distribution of H-bonds over the space of geometrical features. Among all H-bonds that were initially identified by loose geometrical criteria, there are many cases in which a bond critical point was not found between the hydrogen and acceptor atoms.

The distribution of H-bonds over four geometrical parameters are plotted as histograms in Fig. S1 (ESI†). It is evident that in the space of geometrical features, there is not a consistent strict decision line to discriminate topologically identified H-bonds from unidentified cases, although tightening the values of geometrical thresholds can improve the level of agreement. The geometrical threshold values were tightened in the motif assignment step to obtain the greatest possible consistency between the relative stabilities of different conformers and their assigned motifs while maintaining all topologically approved H-bonds in the set of geometrically identified H-bonds. Accordingly, there are three sets of H-bonds in this work: the set of H-bonds initially identified by loose geometrical criteria is denoted as S^{loose}; a subset of it obtained by tightening the geometrical criteria denoted as S^{tight}; and the set of topologically

Table 1 H-bond motifs, populations, relative conformational energy terms and equilibrium constants of all conformers of **MBP** and low-lying conformers of **HEDP**. All energetic values are in kcal mol^{-1} and are relative to the **C1** conformer at each protonation state

Conformer	Motif	Pop. (%)	E_{tot}	E_{gas}	ΔG_{solv}	E_{ZPE}	G_{therm}	K	K^{elec}	K^{vib}	K^{rot}
MBP-HL											
C1	**M1**	100.0	0.00	0.00	0.00	0.00	0.00	1.00	1.00	1.00	1.00
C2	—	0.0	12.30	24.82	−12.71	0.19	−0.26	0.00	0.00	1.93	1.10
C3	—	0.0	13.16	23.25	−10.36	0.27	−0.36	0.00	0.00	2.65	1.09
C4	—	0.0	13.59	23.54	−10.09	0.14	−0.28	0.00	0.00	1.86	1.08
MBP-H_2L											
C1	**M1**	100.0	0.00	0.00	0.00	0.00	0.00	1.00	1.00	1.00	1.00
C2	**M2**	0.0	6.69	13.32	−6.11	−0.52	−1.19	0.00	0.00	2.86	1.09
C3	**M2**	0.0	6.89	14.97	−7.52	−0.56	−1.11	0.00	0.00	2.33	1.10
C4	**M2**	0.0	6.92	15.34	−7.88	−0.53	−1.08	0.00	0.00	2.29	1.09
C5	**M3**	0.0	8.11	9.28	−0.79	−0.38	−0.87	0.00	0.00	2.17	1.06
C6	**M4**	0.0	12.70	19.29	−5.86	−0.73	−1.70	0.00	0.00	4.67	1.09
C7	—	0.0	13.87	29.26	−14.15	−1.24	−2.91	0.00	0.00	14.27	1.19
C8	—	0.0	13.90	27.61	−12.48	−1.23	−2.95	0.00	0.00	15.65	1.16
HEDP-HL											
C1	**M1**	50.8	0.00	0.00	0.00	0.00	0.00	1.00	1.00	1.00	1.00
C2	**M2**	34.4	0.62	3.94	−2.48	−0.84	−1.23	0.68	0.35	1.94	1.00
C3	**M1**	14.2	0.87	0.81	0.04	0.02	−0.10	0.28	0.23	1.21	1.00
C4	**M3**	0.2	3.70	6.50	−2.54	−0.26	−0.66	0.00	0.00	1.97	0.99
C5	**M4**	0.3	3.94	7.58	−3.11	−0.54	−1.40	0.00	0.00	4.25	1.00
C6	**M4**	0.0	5.07	9.63	−4.07	−0.49	−1.05	0.00	0.00	2.59	1.00
C7	**M4**	0.0	5.52	14.17	−8.58	−0.07	−0.25	0.00	0.00	1.37	1.00
HEDP-H_2L											
C1	**M1**	56.8	0.00	0.00	0.00	0.00	0.00	1.00	1.00	1.00	1.00
C2	**M1**	26.4	0.40	2.36	−1.95	−0.01	0.05	0.46	0.51	0.91	1.00
C3	**M1**	16.7	0.71	3.59	−2.74	−0.14	−0.12	0.29	0.30	0.97	1.00
C4	**M2**	0.1	4.51	8.02	−3.18	−0.33	−0.66	0.00	0.00	1.64	1.05
C5	**M2**	0.0	5.66	10.11	−4.26	−0.18	−0.62	0.00	0.00	2.00	1.04
C6	**M2**	0.0	5.81	11.25	−5.00	−0.44	−0.81	0.00	0.00	1.80	1.05
C7	**M3**	0.0	5.89	13.25	−7.26	−0.10	−0.41	0.00	0.00	1.62	1.05
C8	**M4**	0.0	5.97	10.92	−4.79	−0.16	−0.52	0.00	0.00	1.78	1.04

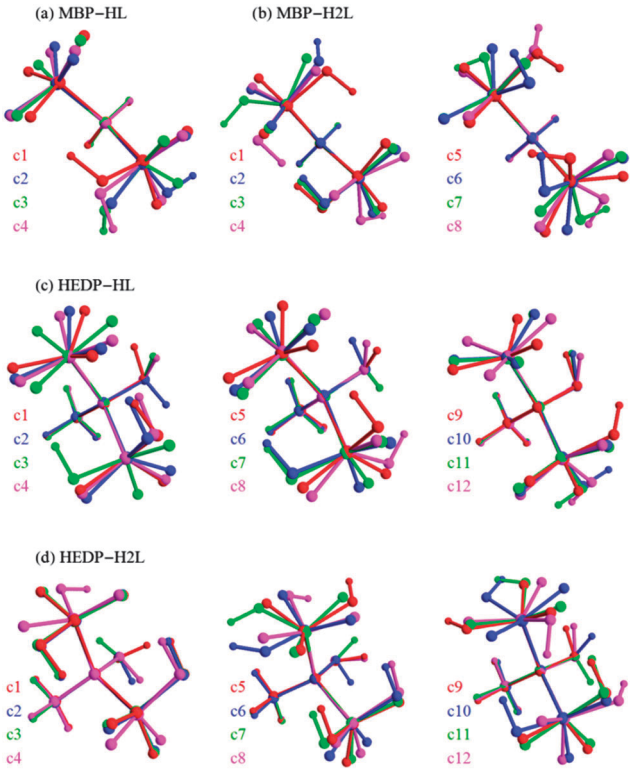

Fig. 2 Optimized geometry of low-lying conformers of **MBP** and **HEDP**. All structures were aligned from their P–C–P backbone.

identified H-bonds, S^{top}, which is a subset of S^{tight}. In other words, we have $S^{top} \subseteq S^{tight} \subseteq S^{loose}$, where the equality holds only for the **MBP-H_2L** subset of data. All motif definitions in the following discussions are based on the S^{tight} set of H-bonds.

3.1. Conformers and H-bonding motifs

As can be seen in Table 1, the relative stabilities of the different conformers are mainly controlled by the electronic part of the partition function. The rotational part is nearly the same for all conformers since the formation of H-bonds does not considerably change the compactness of conformers. On the other hand, the vibrational part acts in the opposite direction of the electronic factor in most cases, but is not dominant. From an entropic point of view, the formation of strong H-bonds is not favored by vibrational degrees of freedom. Accordingly, the conformers are populated by enthalpic (electronic) preference, while entropic (vibrational) effects act in the opposite direction. The general trend for all conformers in Table 1 and Tables S1, S2 (ESI†) is that the solvation stabilizes higher conformers (with weaker or no H-bonds) more than lower conformers (with stronger H-bonds). From the charge separation point of view, this is an expected result since the intermolecular H-bonds act themselves as a stabilizing factor, and the solvent stabilization role becomes less important. Both the **HL** and **H_2L** forms of **MBP** have a single populated conformer (**C1**) at 298 K, while both forms of **HEDP** are mixtures of three conformers at the same conditions. In their analysis of the pH-dependent protonated conformers of **HEDP** using FT-Raman spectroscopy and DFT calculations, Cukrowski and co-workers[15] found two conformers for each of the **HL** and **H_2L** forms of **HEDP**. The molecular mechanical prescreening of the conformational space and the shortcoming of DFT methods in complex H-bonding systems might explain their loss of many conformers that are reported in the present study. The singly populated **HL** and **H_2L** conformers reported in ref. 15 are the same as the most stable conformers **HL-C1** and **H_2L-C1** obtained in the present study for **HEDP**; however, the current analysis shows that each of these conformers has a population around 50%. In the case of **MBP**, the motif-based analysis of different conformers provides a clear explanation of their relative energies. For **MBP-HL**, only one H-bond is possible, resulting in the **M1** motif in the **C1** conformer. The other three conformers have no H-bonds and minor energy differences due to the relative orientations of the P–OH group. In the case of **MBP-H_2L** motifs, the relative energies in Table 1 are clustered based on their motifs in Table 2. **MBP-H_2L-C1** has two inter-phosphonate reciprocal H-bonds that are locked *via* an eight-membered ring. The next three conformers, **C2**, **C3** and **C4**, have the same motif (**M2**) and similar relative energies. In this motif, there is one inter-phosphonate H-bond, and the orientation of the other P–O–H is responsible for the small energy differences. The next conformer **C5** has motif **M3**, which also has a locked structure as a result of two inter-phosphonate H-bonds; however, the acceptor of the second H-bond is the donator of the first one. This pattern of H-bonding locks both PO–H groups *via* a smaller six-membered ring in comparison to **M1**, but it seems that the formation of the second H-bond is not preferred in the presence of solvation effects. While the gas-phase energy of **C5**–**M3** is lower than the average of the {**C2**, **C3**, **C4**} set (with **M2** motif), the solvation free energy provides more stabilization for these three conformers than in **C5**. The last possible H-bonding motif in **MBP-H_2L** is **M4** in the **C6** conformer with one inter-phosphonate H-bond in which the protonated oxygen is the acceptor and thus is weaker than the H-bond of the **M2** motif. The next two conformers, **C7** and **C8**, have no H-bond and thus no assigned motif. As can be seen in Table 2, the **MBP** motifs are the bases of the **HEDP** motifs. The energy ordering of the identified **HEDP** H-bond motifs is the same as their basic counterparts in **MBP**, and the inter-phosphonate H-bonds are generally stronger than those formed between hydroxyl and phosphonate groups.

The relative stability of low-lying **HEDP** conformers can be consistently explained by the types of H-bonds in their motifs. In the **HL** protonation state, the **M1** motif, in which the hydroxyl H-bond is donated to the more negative phosphonate, is expected to be more favored than the **M2** motif. This is in agreement with the gas-phase energies of the **C1**, **C2** and **C3** conformers. However, the solvation effect, zero point energy and thermal contributions to the free energy stabilize the **M2** motif of the **C2** conformer such that it lies lower than the **C3** one on the total energy scale. The next motif, **M3**, in the **HL** form of **HEDP** belongs to just one conformer, **C4**; its lower stability is attributed to the donation of the hydroxyl H-bond to the same acceptor atom that is also donated by the inter-phosphonate H-bond. Similar conclusions can be drawn from

Table 2 Hydrogen bonding motifs in conformers of **MBP** and **HEDP**. Each phosphonate is represented as a triangle with each edge as one of the oxygen atoms (blue: protonated, red: bare). The hydroxyl group is represented by a circle, and each hydrogen bond is depicted as an arrow

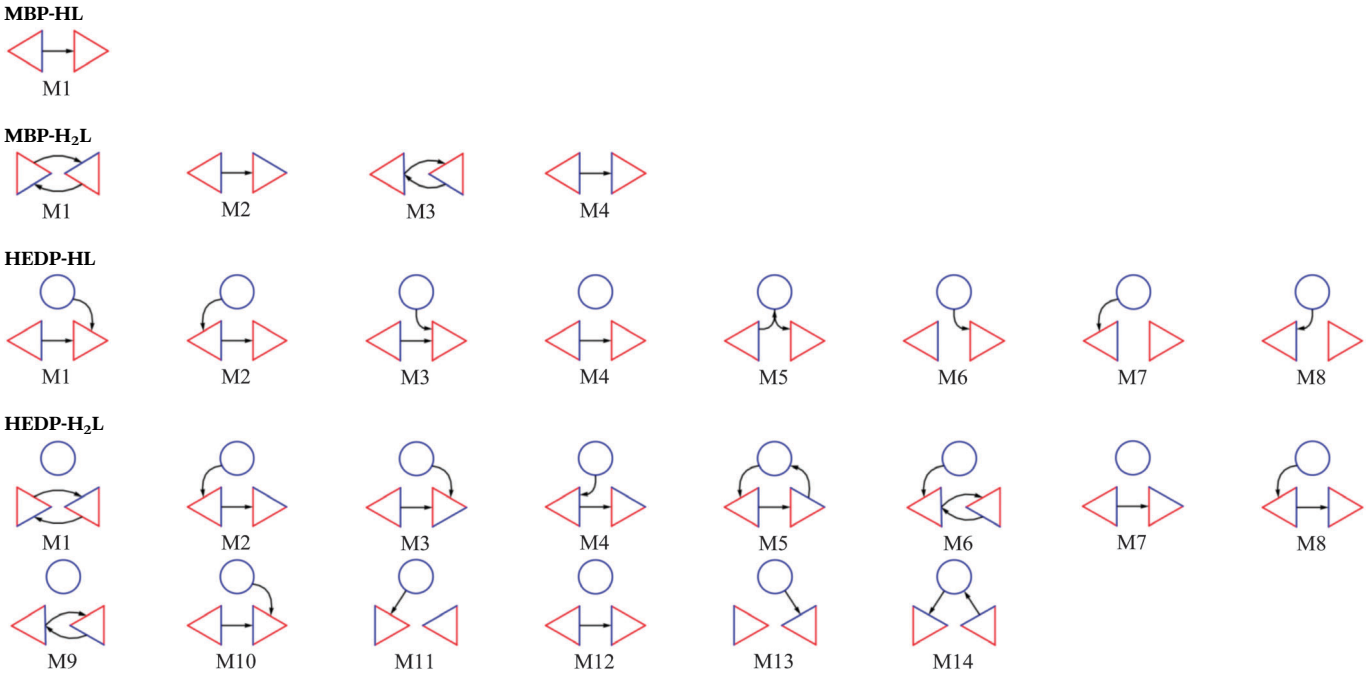

relative stabilities of the **HEDP-H_2L** motifs. The only populated conformers **C1**, **C2** and **C3** share the same motif, **M1**, which keeps the basic inter-phosphonate reciprocal pattern of H-bonds. The orientation of the hydroxyl group is the main factor that controls the energy difference of these three conformers. The presence of the hydroxyl group makes the relative energies spread wider over the energy scale of conformational space, and it is not possible to draw distinct energy borders between different motifs, as in the case of **MBP**.

3.2. H-bond identification and characterization

From a simplistic point of view, all H-bonds in a hydroxy-bisphosphonate moiety can be classified into five types: (i) POH···OP; (ii) POH···O(H)P; (iii) COH···OP; (iv) COH···O(H)P; and (v) POH···O(H)C. However, different conformations, protonation states and H-bonding patterns result in a wide range of values for each characteristic feature, especially the H-bond energy. Before dealing with the QTAIM-derived H-bond energies, it is informative to see how they could be estimated from the relative energies of conformers. The energy differences between the **MBP-HL-C1** conformer and the other three conformers with no H-bonds can be used to estimate the strength of an inter-phosphonate POH···OP H-bond in the **HL** protonation state, which is around 24 kcal mol^{-1} based on gas-phase electronic energies (see Table 1). Each of the similar POH···OP H-bonds in **MBP-H_2L-C1** contribute around 14 kcal mol^{-1} to the stabilization of this conformer with respect to the **C7** and **C8** conformers without H-bonds. The relative gas-phase energies of **C2**, **C3** and **C4** provide nearly the same estimation for a POH···OP H-bond, although it seems to be a little stronger when there is just one H-bond. For the **MBP-H_2L-M3** motif in **C5** (see Table 2), it is not possible to estimate H-bond energies since the H-bonds are asymmetric with respect to the type of donor and acceptor atoms. Qualitatively, it can be said that the POH···OP bond is weaker than it is in **C1** to **C4** but stronger than the other POH···O(H)P bond in the **M3** motif. Indeed, the latter, with an H···O distance of 4.44 au, is much weaker than the similar bond in **MBP-H_2L-C6**, and we can say that both H-bonds in **C5** weaken each other. Finally, the POH···O(H)P in **C6** is estimated to have an energy of around 9 kcal mol^{-1}. These estimates are useful to analyze the consistency of the information on these structures provided by QTAIM. Estimation of H-bond energies from conformational energies is not possible in the case of **HEDP** since no conformer without an H-bond was identified.

Most of the disagreements between the geometrical and topological approaches for H-bond identification correspond to the relation between the hydroxyl group and phosphonate groups, *i.e.*, the existence or absence of a COH···OP or COH···O(H)P H-bond. For example, an energy range of 4.5 to 6.2 kcal mol^{-1} is covered by **HEDP-H_2L** conformers from **C4** to **C11**. This range is wider if one considers their gas-phase relative energies, which are more directly related to the H-bond energies. Any approach to identify H-bonds and quantify their strengths should ultimately be helpful in analyzing such differences in the conformational space of a compound. In the S^{top} set of H-bonds, just one H-bond (an inter-phosphonate one) was detected for **HEDP-H_2L** conformers from **C4** to **C11**. In contrast, in the S^{tight} set of H-bonds, there is an additional H-bond for each of these conformers that results in H-bond motifs **M2**, **M3** and **M4**. As another example, the three **HEDP-HL** conformers **C5**, **C6** and **C7** were assigned to the **M4** motif

without any H-bond between hydroxyl group and any of the phosphonate groups. Such an H-bond is not present in the S^{top} or S^{tight} sets of H-bonds. In these conformers, the hydroxyl group is oriented toward the more negative doubly deprotonated phosphonate group, and this interaction is responsible for the energy difference between these conformers. With a slight variation in the adopted geometrical criteria, one can assign an H-bonds from hydroxyl to phosphonate in the **C5** and **C6** conformers and explain the gas-phase energy differences between these two conformers and the **C7** one. These are some of many examples that show that tunable geometrical criteria are more consistent with the fuzzy nature of H-bond identification than topological analysis, which starts with a true-false step based on the existence or absence of a bond critical point. In other words, the true-false character of topological criteria makes this approach unable to explain diversity in conformational space, while the geometrical criteria can be tuned to satisfactorily describe the origins of energy differences and are a better fit to the fuzzy nature of the problem. This conclusion might be criticized as an unnecessary application of the term ''H-bond'' to what is just a ''weakly attractive H-contact''. However, beyond concern about terminology, where is the rigorous border between these concepts? Here, we think of an H-bond as a concept invented to aid in an explanation, not to rule over it. It will be proposed in the following sections that a quantitative measure of H-bond energy based on the density of potential energy at an ''H-bond'' critical point better predicts the relative stabilities of different conformers when extrapolated to ''weak attractive H-contacts.''

Although many weak H-bonds (or H-contacts) might be ignored by the topological approach, it has the advantage of providing a quantitative scale for the strengths of those that are not ignored. The H-bond energies in Table 3 were calculated *via* an empirical formula (proposed in ref. 38) from QTAIM-derived values of local density of potential energy at H-bond critical points. Interestingly, the results revealed a consistent correlation among the values of E_{HB} in Table 3 and the relative stabilities of **MBP** conformers in Table 1. For example, the **MBP-HL-C1** conformer with just one H-bond is around 24 kcal mol^{-1} lower in gas phase energy than the **C2**, **C3** and **C4** conformers without H-bonds, and the value of E_{HB} for the single H-bond of the **C1** conformer is 23 kcal mol^{-1}. Other values of E_{HB} in **MBP-H_2L** conformers are also in agreement with our previous estimations of H-bond strengths in different motifs based on relative gas-phase conformational energies. In the case of **HEDP**, the relationship between QTAIM-derived H-bond energies and the relative stabilities of conformers becomes somewhat noisy and less evident. There are different reasons for this difference. First of all, as can be seen in Table 3 and Tables S3, S4 (ESI†), many weak hydroxyl-phosphonate H-bonds in **HEDP** are not identified by topological criteria and thus have no value of E_{HB}. These weak interactions affect the relative stabilities of conformers, while their role is not retrieved from topological criteria. Another reason for difference between **HEDP** and **MBP** is the fact that the H-bonding, while still dominant, is not the only factor that determines the relative stabilities. The orientation of the hydroxyl group when it is not involved in an H-bond, the interaction of the methyl group with other structural components and other steric or electronic effects create noise in any strict relationship that one tries to create between H-bond energies and relative conformational stabilities.

3.3. Correlations between H-bond features

Correlations between the geometrical and topological features of H-bonds are of interest to identify and classify different types of H-bonds.[17,18] Ultimately, they could also help derive better scoring formulae for estimating H-bond energies.[19] Important correlations between different features of H-bonds are shown in Fig. 3 and S2 (ESI†). Fitted functional forms and parameters, root mean square error (RMSE) and the coefficient of determination (r^2) for all lines or curves in these figures are reported in Table S5 (ESI†). From the energetic point of view, the most important correlation found in current study is that between H-bond energies (E_{HB}) derived from local density of potential energy (V_{bc}) and the hydrogen-acceptor distance (R_{HA}). We postpone the discussion of this relationship until the next section and deal here with other regular trends between H-bond features. Among geometrical features, the hydrogen-acceptor distance shows better correlations with other features. The reciprocal relation between R_{HA} and R_{DH} in Fig. 3a failed to fit with an inverse or exponential equation. Instead, as can be seen in Fig. S2 (ESI†), there is a nearly linear relation between R_{DH} and $R_{HA}{}^{-6}$. On the other hand, the electron density ρ_{bc} and its Laplacian L_{bc} at the bond critical point show strong correlations with R_{HA} over the entire range of H-bond strength. The reciprocal

Table 3 Hydrogen bond properties in all conformers of **MBP**. All values are in atomic units except E_{HB}, which is in kcal mol^{-1}

	D	A	E_{HB}	R_{DH}	θ_{DHA}	R_{HA}	R_{DA}	ρ_{bc}	L_{bc}	ρ_{rc}	L_{rc}	V_{rc}
MBP-HL												
C1	O11	O23	23.0	1.951	169.4	2.867	4.798	0.0690	0.1507	0.0168	0.0820	0.0162
MBP-H_2L												
C1	O21	O13	10.4	1.878	156.2	3.354	5.128	0.0364	0.1198	0.0149	0.0677	0.0138
C1	O11	O23	10.2	1.877	156.1	3.361	5.135	0.0361	0.1188	0.0148	0.0683	0.0139
C2	O11	O23	11.3	1.878	158.3	3.288	5.081	0.0390	0.1279	0.0146	0.0687	0.0137
C3	O11	O22	10.7	1.875	157.0	3.331	5.109	0.0371	0.1236	0.0145	0.0676	0.0135
C4	O21	O13	10.9	1.876	157.4	3.313	5.097	0.0379	0.1252	0.0146	0.0692	0.0139
C5	O11	O23	8.4	1.863	144.2	3.557	5.185	0.0304	0.1072	0.0153	0.0685	0.0144
C5	O21	O11	2.9	1.838	127.9	4.441	5.756	0.0119	0.0465	0.0105	0.0478	0.0093
C6	O11	O21	6.2	1.845	139.8	3.718	5.264	0.0234	0.0937	0.0120	0.0572	0.0110

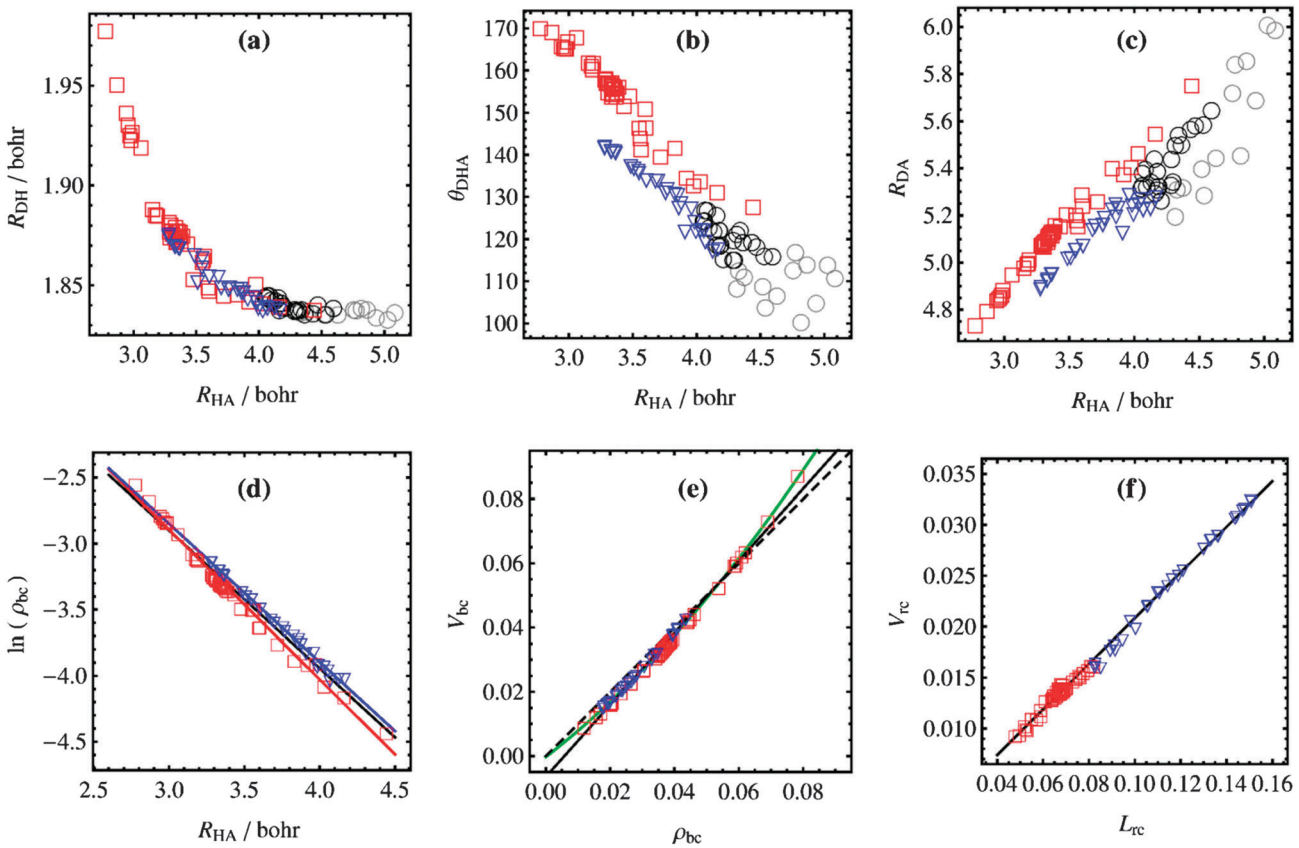

Fig. 3 Important correlations between different features of hydrogen bonds. Red squares: inter-phosphonate H-bonds in S^{top}; blue triangles: hydroxyl-phosphonate H-bonds in S^{top}; black circles: H-bonds in S^{tight} but not in S^{top}; gray circles: H-bonds in S^{loose} but not in S^{tight}. The black, red and blue lines represent linear fits of all, inter-phosphonate data and hydroxyl-phosphonate data, respectively. Green curve: quadratic fit of all data. All values are in atomic units.

relation between ρ_{bc} and R_{HA} has an exponential form, and its parameters are less dependent on the type of donor and acceptor atoms and the H-bonding motif. The relations between local density of potential energy and the electron density at bond or ring critical points are similar, and most data are near the $V = \rho$ line. However, a better regression was obtained for a quadratic relation. There are also strong linear relations between some features obtained at ring critical points. The best example is the linear fit of V_{rc} against L_{rc}, as shown in Fig. 3f with an r^2 value of 0.9959 over the entire set of data. It should be noted that features calculated at ring critical points are not related to the strengths of H-bonds, but can discriminate the inter-phosphonate H-bonds from the hydroxyl-phosphonate cases.

Another interesting quantity is the IR frequency shift of donor–hydrogen bond $\Delta\nu$ implied by H-bonding. In Fig. 4, important correlations between this feature and R_{DH}, R_{HA} and E_{HB} are depicted in different panels. To define frequency shift, the O11–H11 bond in **HEDP-HL-C21** and the OB–HO bond in **HEDP-HL-C5** were chosen as references for PO–H and CO–H bonds, respectively. These bonds participate in no H-bonds, and their frequencies are large enough to act as references for red-shifting H-bonds in the current study. However, it should be noted that since the H-bonds under study are of similar types and among similar donor and acceptor atoms, the resulting correlations also exist for raw values of frequencies without such an offsetting by reference bonds. As can be seen in Fig. 4, the donor-hydrogen distance shows a strong linear correlation with frequency shift, whereas the hydrogen-acceptor distance was not related to frequency shift by any of the examined simple functional forms. In previous studies, considerable correlations were found between the strengths of H-bonds and their frequency shifts.[19] The linear regressions obtained between the topological H-bond energy E_{HB} and $\Delta\nu$ are in agreement with those findings and provide another support for E_{HB} values as measures of H-bond strength. However, it could be interesting to identify the range of values in which a non-topological parameter might disagree with the topological approach for identifying H-bonds. For the frequency shift parameter, this range is represented by the narrow pink region in Fig. 4. The magnitude of this range is defined as $|\Delta\nu_{min}^{top} - \Delta\nu_{max}^{no\text{-}top}| \approx 80\ cm^{-1}$, where $\Delta\nu_{min}^{top} \approx -40\ cm^{-1}$ is the minimum frequency shift in the set of topologically identified H-bonds, and $\Delta\nu_{max}^{no\text{-}top} \approx -120\ cm^{-1}$ is the maximum frequency shift in the set of H-bonds that are not identified by topological criteria (*i.e.*, those without a bond critical point). This range seems to be small with respect to the entire range of frequency shifts observed in all conformational

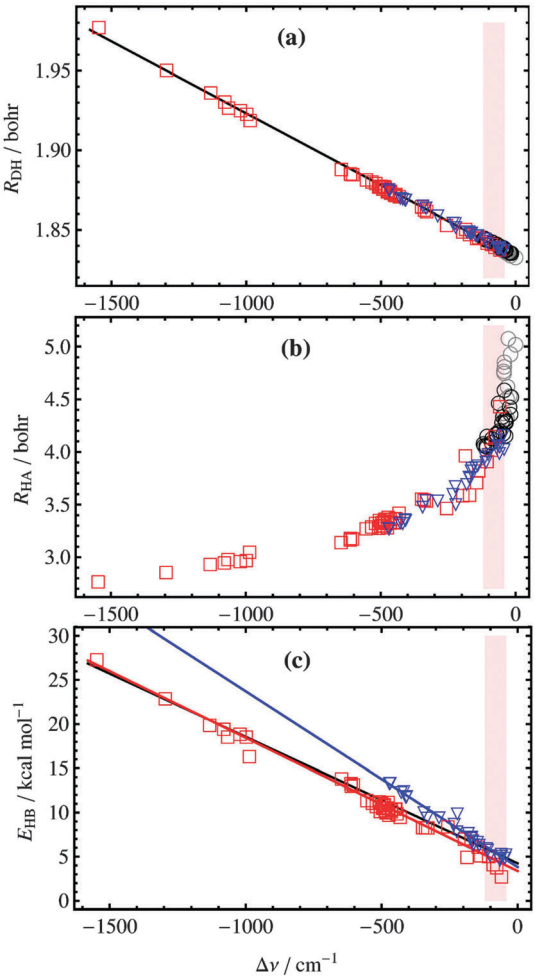

Fig. 4 Correlation of donor-hydrogen bond length, hydrogen-acceptor distance and topological H-bond energy with vibrational frequency shift. Red squares: inter-phosphonate H-bonds in S^{top}; blue triangles: hydroxyl-phosphonate H-bonds in S^{top}; black circles: H-bonds in S^{tight} but not in S^{top}; gray circles: H-bonds in S^{loose} but not in S^{tight}.

space; however, as can be seen in Fig. 4, numerous H-bonds lie in this range and its vicinity. This includes all members of the S^{tight} and S^{loose} sets of H-bonds that are not available in S^{top}. In summary, the topological approach for identifying H-bonds has the advantage of providing a useful quantitative measure of H-bond energy that seems to be consistent with most non-topological measures such as frequency shift and hydrogen-acceptor distance, but it has the critical disadvantage of ignoring many weak H-bonds (or appearance of H-contacts) due to the true-false nature of identification *via* bond critical point. Although weak in strength, these H-bonds play important roles in fine tuning the relative stabilities in the conformational space of a molecule and also in the stabilities of macromolecules such as proteins when one considers their collective effect.

3.4. An H-bond-based model to score conformational stabilities

The best correlation obtained between topological and geometrical features is the inverse dependence of topologically derived

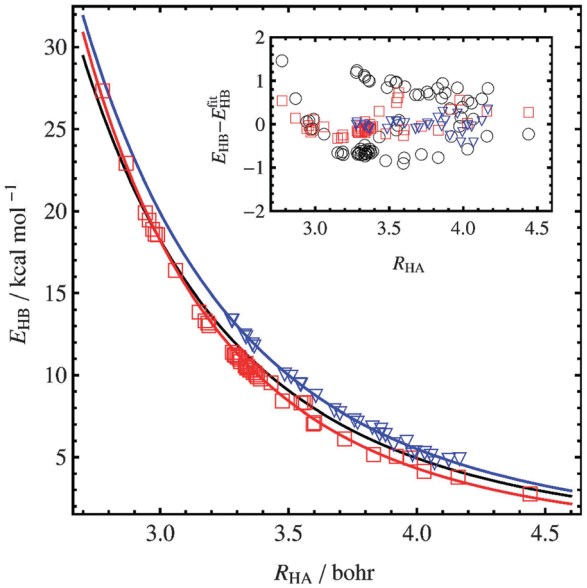

Fig. 5 Dependence of topologically derived H-bond energies on the hydrogen-acceptor distance. Red squares: inter-phosphonate H-bonds in S^{top}; blue triangles: hydroxyl-phosphonate H-bonds in S^{top}. Black, red and blue lines represent an inverse power fit of all, inter-phosphonate and hydroxyl-phosphonate data. Inset plot: fit residuals.

H-bond energy (E_{HB}) on the hydrogen-acceptor distance (R_{HA}). In Fig. 5, values of E_{HB} are plotted against R_{HA} for cases that have a bond critical point (*i.e.*, the S^{top} set of H-bonds). Among the different models that were examined, the best fit of data points in this figure was obtained *via* an inverse power model of the following form:

$$E_{HB} = a/R_{HA}^{n} \quad (7)$$

where different values of parameters a and n were obtained for the entire dataset and different subsets of data (see Table S5, ESI†). Both inter-phosphonate (n = 5.001) and hydroxyl-phosphonate (n = 4.466) sets of H-bonds were fitted by the same r^2 value of 0.9996. The quality of the fit is also reflected by low RMSE values of 0.26 and 0.17 kcal mol^{-1} for inter-phosphonate and hydroxyl-phosphonate sets, respectively. A single fit of all the data will result in a value of 4.539 for n, and the fit quality is decreased with r^2 and RMSE values of 0.9961 and 0.69 kcal mol^{-1}, respectively, which are still quite reasonable. Thus, eqn (7) can reproduce E_{HB} within the chemical accuracy over a wide range of values. The same functional form has been used previously for a large set of intermolecular H-bonds, and an n value of 3.8 was proposed from a single fit of all the data.[19] As a result of diversity of donor and acceptor atoms, the correlation obtained in that work is not as good as what is presented here. Evidently, a single value of n is unable to cover all types of H-bonds in different molecules. According to all of these results, another challenging test could be designed to check the reliability of topologically derived H-bond energies. Assuming that H-bonding is the dominant factor in the energy differences among conformers, and assuming that the eqn (7) can be used to estimate H-bond energy from hydrogen-acceptor distance, the following equation was considered as a

predictive model to estimate the relative stabilities of different conformers:

$$E_{\mathrm{conf}}^{\mathrm{model}} = \alpha + \beta \sum_{i \in S} \left(a_i / R_{\mathrm{HA},i}^{n_i} \right) \quad (8)$$

In this equation, $E_{\mathrm{conf}}^{\mathrm{model}}$ is the model energy of a specific conformer conf $\in \{C1,C2,C3,\ldots\}$ obtained by numeration of its H-bond contributions, and α and β are some constants loosely assumed to be the same for all conformers. The sum is done over all of H-bonds in a conformer that also belong to an S set of H-bonds, which might be any of S^{top}, S^{tight} or S^{loose}. For the case of $S = S^{\mathrm{top}}$ the model predictions are based the existence of an H-bond critical point confirmed by topological criterion; thus, the conformers will be scored by the sum of density of potential energy at their H-bond critical points. On the other hand, when the S set is S^{tight} or S^{loose}, the fitted parameters in eqn (7) are again obtained over the S^{top} set of data, but are used in eqn (8) in an extrapolatory fashion for other cases of H-bonds that have no bond critical point. The best values of parameters α and β were obtained *via* a least squares regression of eqn (8) against calculated *ab initio* conformational energies ($E_{\mathrm{conf}} \equiv E_{\mathrm{tot}}$). The model conformational energies obtained from eqn (8) are plotted against *ab initio* conformational energies in Fig. 6 for **MBP-H$_2$L**, **HEDP-HL** and **HEDP-H$_2$L**. All values in this figure are relative to the **C1** conformer of each system, and the absolute errors of model conformer energies are shown in embedded plots. In the case of **MBP-H$_2$L**, *ab initio* conformational energies are reproduced quite well from the sum of H-bond energies with an RMS error of 0.7 kcal mol^{-1}. The ability of the model is reduced for **HEDP-HL** and **HEDP-H$_2$L** systems. In the case of **HEDP-HL**, the RMS errors are 1.9, 1.7 and 1.5 kcal mol^{-1} for S^{top}, S^{tight} and S^{loose} sets, respectively. Thus, the inclusion of H-bonds without a bond critical point improves the conformational energy predictions. This is even more evident for **HEDP-H$_2$L**; the RMS errors are 2.5, 1.7 and 1.5 kcal mol^{-1} for S^{top}, S^{tight} and S^{loose} sets, respectively. As noted previously, the role of H-bonds in the relative energies of **HEDP** conformers is less dominant in comparison with **MBP**, and the simple model presented by eqn (8) is expected to be less accurate. Factors other than H-bonding that affect the relative stabilities of conformers are implicitly included in this model as parameters α and β, but their role is assumed to be the same for all conformers of a system. Obviously, this is a crude estimate of the roles of non-H-bonding factors such as the orientations of OH groups not involved in H-bonding or other steric or electronic interactions between different structural components such as the methyl, hydroxyl and phosphonate groups. However, the results presented in Fig. 6 show that the H-bond energy estimations provided by the local density of potential energy at the H-bond critical point is a reliable and consistent measure of H-bond strength over the entire conformational space of a molecule. If the correlations and regularities obtained here remain valid in other systems such as peptides, there might be an interesting opportunity for the development of more reliable structural scoring functions based on relations such as eqn (7) after, of course, some careful atom-typing.

4. Summary and conclusion

After more than four decades, therapeutic features of bisphosphonates are still the subject of active research.[40] The extensive conformational search performed in this study resulted in 4, 8, 22 and 37 conformers for **MBP-HL**, **MBP-H$_2$L**, **HEDP-HL** and **HEDP-H$_2$L**, respectively. Free energy calculations including continuum solvation free energies show that at ordinary temperatures, only the most stable conformer (**C1**) is populated in both protonation states of **MBP**, while a mixture of three conformers (**C1**, **C2** and **C3**) is present in the **HEDP** system regardless of protonation state. Possible H-bonding motifs were defined and assigned to each conformer to analyze the role of H-bonds in the conformational diversity of a hydroxy-bisphosphonate moiety. Inter-phosphonate H-bonding was found to be preferred over hydroxyl-phosphonate H-bonding patterns, especially in the **HL** protonation state.

Two different approaches based on topological and geometrical criteria were compared with each other in the identification and

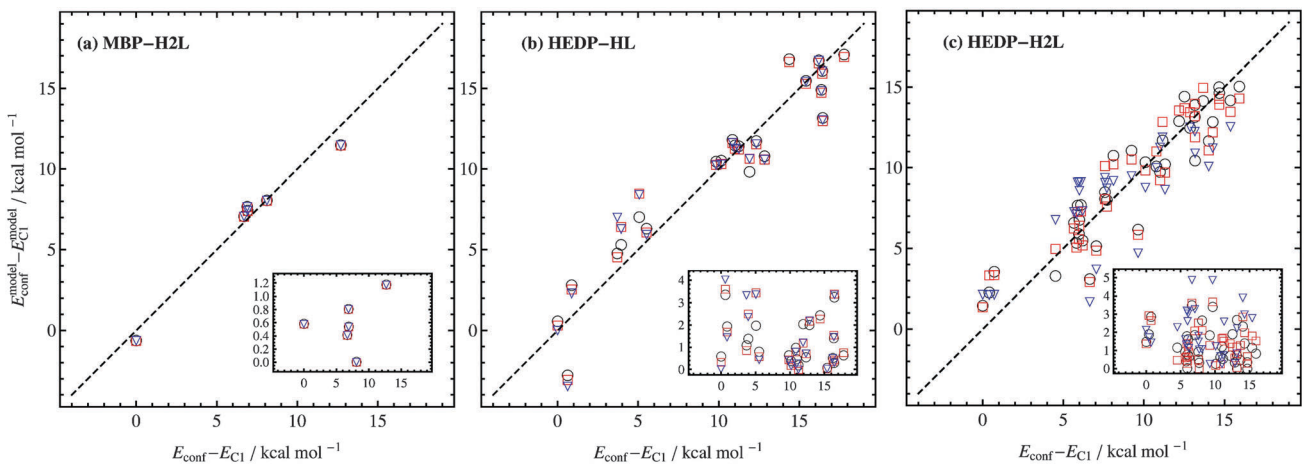

Fig. 6 H-bond-based prediction of relative conformational energies ($E_{\mathrm{conf}}^{\mathrm{model}}$) in comparison with their calculated *ab initio* values ($E_{\mathrm{conf}} \equiv E_{\mathrm{tot}}$). Blue triangles: S^{top} set of H-bonds; red squares: S^{tight} set of H-bonds; black circles: S^{loose} set of H-bonds. Inset plots: prediction errors in kcal mol^{-1}.

characterization of H-bonds. The most important correlations between H-bond features were analyzed within or between each of these approaches. Among geometrical parameters, the hydrogen-acceptor distance exhibits the best correlations with other parameters. Among topological features, the potential energy density at the H-bond critical point and the electron density itself are possible candidates for the construction of regular relationships for the characterization of H-bonds. As a result of the true-false nature of critical point identification, numerous weak H-bonds over the conformational space are ignored in topological analysis. Though weak in strength, these H-bonds play an important role in fine tuning the relative stabilities of different conformers. The tunable character of geometrical features or other non-topological measures such as the magnitude of frequency shift seems to provide a better handling of the fuzzy nature of the H-bond identification problem.

On the other hand, besides the initial identification stage, the topological approach has the advantage of providing a useful quantitative measure to estimate H-bond strength from local density of potential energy at the H-bond critical point. It was shown that there is a strong correlation between this topologically derived H-bond energy and the hydrogen–acceptor distance. Without an intercept parameter, an inverse power functional form was used to represent this correlation, and the prediction errors remain around a fraction of 1 kcal mol^{-1} over a wide range of energy values. By extrapolating this relation to the set of topologically unidentified weak H-bonds, a simple model was proposed that estimates the relative stabilities of conformations from their hydrogen-acceptor distances. Although this model is based on a crude assumption about the role of other factors in relative conformational stabilities, its reasonable accuracy shows the consistency of topologically derived measures of H-bond energy.

References

1 R. Graham and G. Russell, Bisphosphonates, *Bone*, 2011, **49**, 2.
2 M. J. Rogers, J. C. Crockett, F. P. Coxon and J. Mönkkönen, *Bone*, 2011, **49**, 34.
3 F. H. Ebetino, C. N. Roze, C. E. McKenna, B. L. Barnett, J. E. Dunford, R. G. G. Russell, G. E. Mieling and M. J. Rogers, *J. Organomet. Chem.*, 2005, **690**, 2679.
4 S. B. Gabelli, J. S. McLellan, A. Montalvetti, E. Oldfield, R. Docampo and L. M. Amzel, *Proteins: Struct., Funct., Bioinf.*, 2006, **88**, 62.
5 F. Yin, R. Cao, A. Goddard, Y. Zhang and E. Oldfield, *J. Am. Chem. Soc.*, 2006, **128**, 3524.
6 S. Mukherjee, Y. Song and E. Oldfield, *J. Am. Chem. Soc.*, 2008, **130**, 1264.
7 J. E. Dunford, A. A. Kwaasi, M. J. Rogers, B. L. Barnett, F. H. Ebetino, R. G. G. Russell, U. Oppermann and K. L. Kavanagh, *J. Med. Chem.*, 2008, **51**, 2187.
8 E. Kotsikorou and E. Oldfield, *J. Med. Chem.*, 2003, **46**, 2932.
9 E. Matczak-Jon and V. Videnova-Adrabinska, *Coord. Chem. Rev.*, 2005, **249**, 2458.
10 I. Cukrowski, L. Popovic, W. Barnard, S. O. Paul, P. H. van Rooyen and D. C. Liles, *Bone*, 2007, **41**, 668.
11 J. P. Rasanen, E. Pohjala and T. A. Pakkanen, *J. Chem. Soc., Perkin Trans. 2*, 1996, 39.
12 J. P. Rasanen, E. Pohjala, H. Nikander and T. A. Pakkanen, *J. Phys. Chem.*, 1995, **100**, 8230.
13 J. Robinson, I. Cukrowski and H. M. Marques, *J. Mol. Struct.*, 2006, **825**, 134.
14 K. Ohno, K. Mori, M. Orita and M. Takeuchi, *Curr. Med. Chem.*, 2011, **18**, 220.
15 W. Barnard, S. O. Paul, P. H. van Rooyen and I. Cukrowski, *J. Raman Spectrosc.*, 2009, **40**, 1935.
16 M. Arabieh, M. H. Karimi-Jafari and M. Ghannadi-Maragheh, *J. Mol. Model.*, 2013, **19**, 427.
17 T. Steiner, *Angew. Chem., Int. Ed.*, 2002, **41**, 48.
18 S. J. Grabowski, *J. Phys. Org. Chem.*, 2004, **17**, 18.
19 K. Wendler, J. Thar, S. Zahn and B. Kirchner, *J. Phys. Chem. A*, 2010, **114**, 9529.
20 G. Hagele, Z. Szakacs, J. Ollig, S. Hermens and C. Pfaff, *Heteroat. Chem.*, 2000, **11**, 562.
21 V. Barone and M. Cossi, *J. Phys. Chem. A*, 1998, **102**, 1995.
22 M. Cossi, N. Rega, G. Scalmani and V. Barone, *J. Comput. Chem.*, 2003, **24**, 669.
23 R. A. Pierotti, *Chem. Rev.*, 1976, **76**, 717.
24 F. Floris and J. Tomasi, *J. Comput. Chem.*, 1989, **10**, 616.
25 P. Su and H. Li, *J. Chem. Phys.*, 2009, **130**, 074109.
26 R. M. Balabin, *J. Chem. Phys.*, 2008, **129**, 164101.
27 R. M. Balabin, *Mol. Phys.*, 2011, **109**, 943.
28 T. H. Dunning Jr., *J. Chem. Phys.*, 1989, **90**, 1007.
29 D. E. Woon and T. H. Dunning Jr., *J. Chem. Phys.*, 1993, **98**, 1358.
30 A. Halkier, T. Helgaker, P. Jørgensen, W. Klopper and J. Olsen, *Chem. Phys. Lett.*, 1999, **302**, 437.
31 T. Helgaker, W. Klopper, H. Koch and J. Noga, *J. Chem. Phys.*, 1997, **106**, 9639.
32 D. G. Truhlar, *Chem. Phys. Lett.*, 1998, **294**, 45.
33 M. W. Schmidt, K. K. Baldridge, J. A. Boatz, S. T. Elbert, M. S. Gordon, J. J. Jensen, S. Koseki, N. Matsunaga, K. A. Nguyen, S. Su and T. L. Windus, *et al.*, *J. Comput. Chem.*, 1993, **14**, 1347.
34 D. A. McQuarrie, *Statistical Mechanics*, HarperCollins, New York, 1976.
35 R. Chelli, F. L. Gervasio, C. Gellini, P. Procacci, G. Cardini and V. Schettino, *J. Phys. Chem. A*, 2000, **104**, 11220.
36 A. Bondi, *J. Phys. Chem.*, 1964, **68**, 441.
37 P. Popelier, *Prentice-Hall*, Englewood Cliffs, NJ, 2000.
38 E. Espinosa, E. Molins and C. Lecomte, *Chem. Phys. Lett.*, 1998, **285**, 170.
39 F. Biegler-König, J. Schönbohm and D. Bayles, *J. Comput. Chem.*, 2001, **22**, 545.
40 Y.-L. Liu, R. Cao, Y. Wang and E. Oldfield, *ACS Med. Chem. Lett.*, 2015, **6**, 349.

